JOURNAL OF COMPUTATIONAL PHYSICS 119, 156–163 (1995)

A Single Ray Approximation for α Particle Transport

J. P. APRUZESE, R. W. CLARK, AND J. W. THORNHILL

Radiation Hydrodynamics Branch, Plasma Physics Division, Naval Research Laboratory, Washington, DC 20375

Received April 25, 1994; revised September 28, 1994

We report the development of a one-ray approximation for the numerical transport of 3.5 MeV α particles generated in DT fusion reactions. Similar in spirit to techniques used in photon transport, this method provides respectable accuracy at potentially large savings in time and storage when compared to multigroup diffusion, S_n, or Monte Carlo techniques. The approximation works in a restricted, but large, class of plasmas, those in which scattering of the α's and bending of their trajectories by magnetic fields can be neglected. Test cases in planar, cylindrical, and spherical geometry are presented. In another calculation it is demonstrated that the achievement of ignition in an imploding Z pinch may depend sensitively on the degree to which a magnetic field confines the α particles in the dense central core.

1. INTRODUCTION

In high density laboratory fusion plasmas, the principal bootstrap mechanism by which the energy of the fusion products is recaptured by the plasma is the deposition by Coulomb collisions of the 3.5 MeV initial energy of the α particles formed in DT fusion. Of course, the fundamental physics of the stopping of these particles has long been well characterized [1–4]. For electron temperatures below ~25 keV, the deposition to electrons dominates, except near the end of the α trajectory. At higher temperatures, ion stopping is significant throughout the α particle path and scattering of the α's becomes significant. Precise numerical simulation of these effects requires the use of detailed methods which follow the degradation of the α-particle energy and the resulting changes in ion and electron stopping due to both the energy reduction and variations in the overall plasma conditions as a function of space and time. Examples of such approaches are multigroup diffusion [2, 5], S_n methods [1, 6], and Monte Carlo techniques [1, 2].

However, the simulation of fusion plasmas requires modeling of a large variety of diverse physical processes arising from hydrodynamic motion, radiation, and plasma effects and their associated instabilities. Any approximation technique or simplifying insight for the relatively well-characterized mechanism of α transport is welcome in that the computational resources will be freed for more realistic characterization of less well understood physics. It is the purpose of this paper to present such a simplification. In succeeding sections, a new transport algorithm for DT-produced α particles is described. This method is based on a one-ray approximation and has been employed for test cases in spherical, cylindrical, and planar geometry. It is valid for plasmas in which the α trajectories may be reasonably approximated as straight lines. There is generally no magnetic field present in spherical laser-imploded pellets. Also, Kalantar and Hammer [7] have recently presented experimental evidence that the current in wire-initiated dense Z pinches flows predominantly on the surface of the outer coronal plasma. In the dense interior of such a pinch there will be no magnetic field. However, the transport method to be presented cannot treat the recapture of orbiting α's, which may be important in some cases as found by Lovberg [8]. Nor is it appropriate for tokamaks and related magnetic fusion reactors or the simulation of anomalous transport. Comparisons are made to results obtained from a Monte Carlo treatment, which is more than three orders of magnitude slower than the presently described single angle method. Finally, we evaluate the potential for ignition in an imploding Z pinch driven by a current of 120 MA, under the contrasting assumptions of local deposition of the entire 3.5 MeV, or free-streaming nonlocal α transport.

2. METHODS OF CALCULATION

2.1. *An Overview of the Single Ray Approach*

This method employs a geometrical setup similar to that described in Refs. [9, 10] for photon transport. The medium—planar, cylindrical, or spherical—is divided into a number of finite-sized cells (rather than grid points). From the midpoint of each cell a ray is traced in both the positive and negative directions at an angle $\bar{\theta}$ to the local outward drawn radius or normal. Using an approximate solution of the stopping power equation along the ray, one then determines what fraction of the birth energy of 3.5 MeV is deposited in each cell intersected by the ray. The fraction of 3.5 MeV deposited in cell j by an α particle born in cell i is referred to as the "coupling constant" U_{ij}. Calculation of the matrix U_{ij} characterizes the α transport within the limits of using a finite number of cells to represent the medium.

In planar geometry, a ray originating in a given cell intersects all other cells, and the calculation of the U_{ij} is straightforward.

0021-9991/95 $6.00

However, in cylindrical or spherical geometry, only cells lying further from $r = 0$ than the originating cell are guaranteed to be intersected by the ray (although many inner cells will in practice usually be intersected). In these geometries, therefore, the inner-to-outer coupling constants (U_{ji}, where $j \geq i$, inner cells labeled with lower numbered indices) are calculated directly with the stopping power equation, whereas the U_{ji}, outer-to-inner constants, are obtained via a reciprocity relation which is given below.

2.2. *Details of the Single Ray Approach*

As mentioned above, the slowing of α particles is dominated by electrons at temperatures $\leq$25 keV, suggesting that an approximation for this temperature range can be based on the following hierarchy: initially ignore ion stopping and apply a corrective term to the resulting algorithm. A similar corrective approach to the treatment of ion stopping was employed in Ref. [4]. The stopping of 3.5 MeV α particles by electrons is described by Eq. (3a) of Ref. [1], viz.,

$$\frac{dE}{dx} = -aE^{1/2}, \tag{1}$$

where

$$a = -\frac{23.2\rho}{T_e^{3/2}}\left[1 + 0.17 \ln\left(\frac{T_e}{\rho^{1/2}}\right)\right], \tag{2}$$

E is the α energy divided by 3.5 MeV, ρ is the density divided by the DT solid density, and T_e is the electron temperature in thousands of electron volts. The quantity a does not depend on the energy of the α particle during slowdown, and it is constant within each cell, although varying, in general, from cell to cell. The fact that a is independent of the energy facilitates the numerical solution without recourse to a multigroup method, which is an important aspect of the efficiency of this method. Defining a stopping coefficient $k = a/2$, the solution to Eq. (1) is

$$E_0^{1/2} - E^{1/2} = k\Delta x. \tag{3}$$

In Eq. (3), E_0 is the energy of the α particle as it enters the cell of thickness Δx, and E is its energy upon exiting. If ion stopping is negligible and one is interested only in computing the energy deposited along a prescribed path, Eq. (3) can be used to obtain the U_{ij} by assuming the equal probability of emission in each direction along the ray extending from the point of origin of the particle. However, for most applications of interest, we must consider the choice of an average angle to represent multidirectional deposition, as well as a technique to correct for ion stopping.

As regards the choice of an effective angle, there is no single value which is optimum for all conditions. For instance, an angle, which might do well in representing energy deposition near the point of birth of the α particle, would do poorly at large separation. The best justification for any such choice is the degree of agreement obtained with multiangle methods. Consider the traversal of a slab or thin spherical shell by an α particle of initial energy 3.5 MeV. If the thickness of the layer is Δx, the angle of the particle's path relative to the local normal or radius is θ, and $\mu = \cos\theta$, the decrement in the square root of the energy across the layer is, according to (3),

$$\Delta E^{1/2} = \frac{k\Delta x}{\mu} \equiv \frac{\tau_0}{\mu}, \tag{4}$$

letting $E = 1$ correspond to the birth energy of 3.5 MeV, $\Delta E^{1/2} = 1 - E^{1/2}$, and $\Delta E = 1 - E$. The fundamental importance of the decrement of the square root of the energy in the α transport has been previously demonstrated elsewhere (see Eq. (10) of Ref. [4]). Squaring both sides of Eq. (4) yields

$$\Delta E(\tau_0, \mu) = \tau_0\left(\frac{2}{\mu} - \frac{\tau_0}{\mu^2}\right). \tag{5}$$

Equations (4) and (5) apply only for $\tau_0 < 1$ and $\mu > \tau_0$. If $\mu \leq \tau_0$ or $\tau_0 \geq 1$ the particle is stopped in the layer ($\Delta E = 1$). The angle-averaged decrease in the energy during traversal of the layer is, assuming isotropic angular distribution,

$$\overline{\Delta E}(\tau_0) = \tau_0 + \int_{\tau_0}^{1} \Delta E(\tau_0, \mu)\, d\mu = \tau_0^2 - 2\tau_0 \ln \tau_0. \tag{6}$$

By equating the right-hand sides of Eqs. (5) and (6), for any $\tau_0 < 1$ an effective $\overline{\mu} = \cos\overline{\theta}$ may be found such that $\Delta E(\tau_0, \overline{\mu}) = \overline{\Delta E}(\tau_0)$. For example, at $\tau_0 = 0.5$, $\overline{\Delta E} = 0.94$, indicating that 94% of the energy of a sample of α particles emitted isotropically at the edge of such a layer would be absorbed within the layer. To match this absorption at a single angle requires $\overline{\mu} = 0.66$. However, this choice of $\overline{\mu}$ would not be optimum for transport calculations. For thinner layers, absorption would be seriously underpredicted. At $\tau_0 = 0.04$, $\overline{\Delta E} = 0.26$, but using $\overline{\mu} = 0.66$ would yield a fractional deposition of only 0.12. On an angle-averaged basis, 50% absorption of the energy of the α particle occurs at $\tau_0 = 0.11$, but using $\overline{\mu} = 0.66$ yields only 31% absorption. Our choice of $\overline{\mu}$ is 0.38, which matches the 50% deposition point at $\tau_0 = 0.11$ exactly, and is found to provide satisfactory agreement with more accurate calculations. This is not surprising, since if the deposition is matched precisely at the energy midpoint of the trajectory, one expects reasonable agreement to occur along those portions of the path where the bulk of the energy is deposited. At $\tau_0 = 0.04$, $\overline{\mu} = 0.38$ predicts 20% absorption instead of the exact 26%. For $\tau_0 = 0.25$, the correct deposition fraction is 0.76, whereas $\overline{\mu} = 0.38$ yields 0.88. Even at $\tau_0 = 0.5$, where the correct angle-averaged absorption fraction is 0.94, the use of $\overline{\mu} = 0.38$ predicts 1.0 (full stopping). The deposition fraction

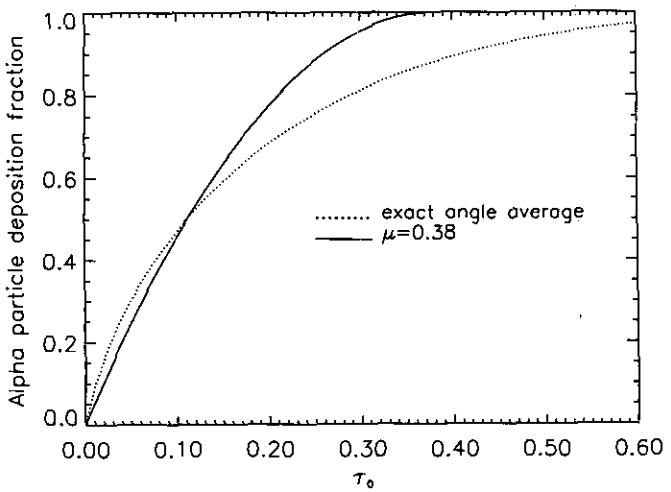

FIG. 1. Fraction of 3.5 MeV α particle energy deposited is plotted vs the absorption thickness of a planar layer, as described in the text. Both the exact angle-averaged solution and the result for $\cos\bar{\theta} = 0.38$ are shown.

for the relevant τ_0 range is plotted in Fig. 1 for both the exact angle-averaged and $\bar{\mu} = 0.38$ cases.

Use of the μ-integral in the form of Eq. (6) is valid for a slab or a thin spherical shell. In cylindrical geometry an additional complication arises from the elongation in the z direction which results in the more oblique angles having greater solid angle weight than in planar or spherical geometry. The following empirical correction has proven satisfactory. For cylindrical cases, the path segments are computed as if the medium were spherical, and then their lengths are multiplied by 1.3 to account for the greater average trajectory distances due to the greater prevalence of oblique angles.

For spherical and cylindrical cases, the coupling constants for inner-to-outer cells are computed directly using the ray along the mean angle $\cos^{-1}$ (0.38). To obtain the U_{ji}, which are the outer-to-inner couplings, a reciprocity relation which is derived and discussed in Refs. [10, 11] is invoked,

$$U_{ji} = U_{ij}\left[\frac{V_i k_i}{V_j k_j}\right], \tag{7}$$

where, in Eq. (7), the k's are as previously defined and the V's are the volumes of the respective cells. Equation (7) is valid for both particles and photons. In the latter case, the k's are absorption coefficients. If energy is to be conserved, $\sum_j U_{ij}$ should never exceed unity; otherwise unphysical deposition energy will be created. Occasionally, this sum can slightly exceed unity because of either numerical noise or the approximate nature of the method. If this occurs, the sum is renormalized to unity, a simple but effective method of guaranteeing energy conservation.

Equations (2) and (3) describe only the electron stopping of the α's. For temperatures exceeding ~25 keV, ion stopping is important. To calculate this, the full ion stopping term of Eq. (3a) of Ref. [1] can be employed, and this is exactly what is done in the Monte Carlo method described in the next section. Note that for temperatures significantly less than 25 keV, the simplified method takes full account of the electron stopping, which is the major α energy absorption mechanism. The presently described method is optimally employed in modeling plasmas with such temperatures. To allow for ion stopping, we make use of an empirical corrective term for DT given in Ref. [1], in which the fraction of α energy absorbed by the ions is approximated by $f_i = (1 + 32/T_e)^{-1}$. This correction for ion stopping is implemented by multiplying the electron stopping coefficient by $1/(1 - f_i)$ prior to the calculation of the U_{ij}.

2.3. *The Monte Carlo Model*

For comparison with the new method described above, the transport of the alpha particles is separately accomplished using a random trajectory method. It is conceptually very simple, but can be computationally intensive. Given the rate of production of alphas in each spatial zone, a series of alpha particle starting locations and random trajectories is assigned. The starting locations take account of the cell geometry (for example, assuming uniform alpha production within a cell, the probability of an alpha being produced at radius r must satisfy $P(r) \propto r$ in cylindrical geometry, and $P(r) \propto r^2$ in spherical geometry). If R_i is the inner boundary of a spatial zone, R_o is the outer boundary, and $N_k^{[1]}$ is a random number on the interval [0, 1], the initial radial position r_k for the kth trajectory can be written as

$$r_k = [R_i^n + N_k^{[1]}(R_o^n - R_i^n)]^{1/n}, \tag{8}$$

where $n = 1$ for planar geometry, $n = 2$ for cylindrical geometry (axial symmetry), and $n = 3$ for spherical symmetry.

If the alpha particle velocity distribution is isotropic, the random trajectories must be evenly (to within statistical fluctuations) distributed over 4π steradians. For all three geometries (planar, cylindrical, and spherical), the same notation is used to describe the trajectories. Let θ be the polar angle and ϕ be the azimuthal angle. A trajectory with $\theta = 0$ is defined to be normal to the surface in planar geometry and perpendicular to the axis in cylindrical geometry. A uniform distribution thus requires that the polar angle for the kth trajectory be calculated from

$$\sin\theta_k = 2N_k^{[2]} - 1, \tag{9}$$

where $N_k^{[2]}$ is a (second) random number on the interval [0, 1]. Care must be taken in the derivation of $\cos\theta_k$ that negative values are permitted. The azimuthal angle is calculated from

$$\phi_k = 2\pi N_k^{[3]}, \tag{10}$$

where $N_k^{[3]}$ is a (third) random number on the interval [0, 1]. To get accurate statistics, many rays need to be employed. In a typical calculation, 50–200 rays are needed per spatial zone to obtain convergence to 1–2% with a 1000-ray calculation. A 10-ray calculation yields differences of typically ~7%, in accord with the well-known error variation as the inverse square root of the number of rays. Although straight trajectories were assumed in the simulations, the model can easily take magnetic field effects (Larmor orbits) into account. No attempt has been made to model the effects of scattering, so that the alpha particle ranges which are calculated should be considered upper limits.

The collisional stopping powers used in the calculation are taken from Ref. [1, Eq. (3a)]. Both the electron and DT ion stopping terms are included. The energy degradation of the alpha particle and the deposition of energy in each spatial zone that the particle traverses are calculated by dividing the path into a large number of segments, such that the relative energy loss in each segment is small. The spatial zone that the alpha is traversing is determined by calculating the instantaneous radius. If cartesian coordinates are defined for the alpha particle

$$x_k = x_{k0} + S_k \cos\theta_k \cos\phi_k \tag{11a}$$

$$z_k = z_{k0} + S_k \cos\theta_k \sin\phi_k \tag{11b}$$

$$y_k = y_{k0} + S_k \sin\theta_k, \tag{11c}$$

where S_k is the distance transversed by the particle along the trajectory, then the radius is given by

$$r_k = [x_k^2]^{1/2} \quad \text{(planar)} \tag{12a}$$

$$r_k = [x_k^2 + y_k^2]^{1/2} \quad \text{(cylindrical)} \tag{12b}$$

$$r_k = [x_k^2 + y_k^2 + z_k^2]^{1/2} \quad \text{(spherical).} \tag{12c}$$

Since the x-direction is aligned with the polar axis, there is no loss in generality if $y_{k0} = z_{k0} = 0$. In planar geometry, y_{k0} and z_{k0} can be eliminated by translations of the starting position *in the plane*. For cylindrical geometry, they can be eliminated by a translation along the axis and an azimuthal rotation. In spherical geometry, they can be eliminated by two rotations and considerations of symmetry. If and when the calculated radius exceeds the radius of the outer boundary of the plasma, the particle is assumed to have escaped, and calculation of the trajectory ceases. If the energy of the particle drops to zero along a trajectory, it is assumed to have been stopped, and calculation of the trajectory ceases. The energy loss by electron collisions goes into local electron heating, and the loss by ion collisions goes into ion heating.

3. COMPARATIVE CALCULATIONS

3.1. *Tests in Three Geometries*

We have run numerical tests comparing the two methods for a total of approximately 20 different initial conditions in planar, cylindrical, and spherical geometry. A set of three representative calculations, one for each geometry, is presented here. In each case we consider a fully ionized pure DT plasma whose density is fixed in time but whose temperature increases according to and solely due to, the bootstrap heating by 3.5 MeV α particles. Our point of comparison is the temperature as a function of space and time. This is very sensitive to the α transport and the subsequent heating, since the DT fusion reaction is such a strong function of temperature. The DT burn is computed using the burn-up equation [1], with the DT reaction rate coefficient given by the analytic approximation

$$R(\text{cm}^3\,\text{s}^{-1}) = \frac{8.5 \times 10^{-12} T_i^{-2/3} \exp(-21 T_i^{-1/3})}{1 + 0.0045 T_i^{3/2}}, \tag{13}$$

where T_i is the ion temperature in thousands of electron volts. This expression fits the data of Ref. [12] to within a few percent for $T_i < 500$ keV.

The comparative benchmark calculations for planar and cylindrical geometry are shown in Figs. 2 and 3. In each case, the total density is spatially uniform and is fixed at 2.13 g cm^{-3}, 10 times the DT solid density. The thickness of the plane and radius of the cylinder are each 1.0 mm. The initial temperature is 1 keV, except in one of the 10 spatial cells which is set at 5 keV, sufficient to trigger ignition if the density is assumed fixed on a timescale of several nanoseconds. The central cell is chosen for the elevated temperature in the cylinder, and an edge cell is initially hotter in the planar case. As the α particles are emitted from the initially hot region, a burn wave envelops the rest of the medium over 5–10 ns. The detailed comparisons in Figs. 2 and 3 reveal that the single ray approximation tracks

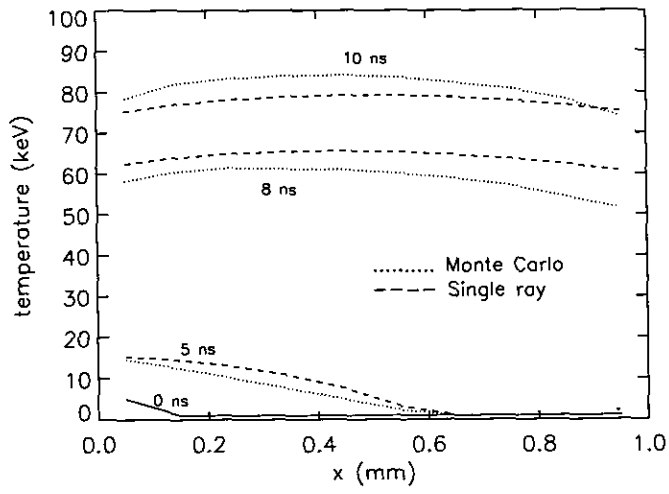

FIG. 2. Ion and electron temperature, assumed equal, are shown as a function of space and time for a pure DT slab of width 1.0 mm, for both the single ray and Monte Carlo calculations. The density is assumed fixed at 2.13 g cm^{-3}, and the temperature rises in accordance with bootstrap heating by the α's.

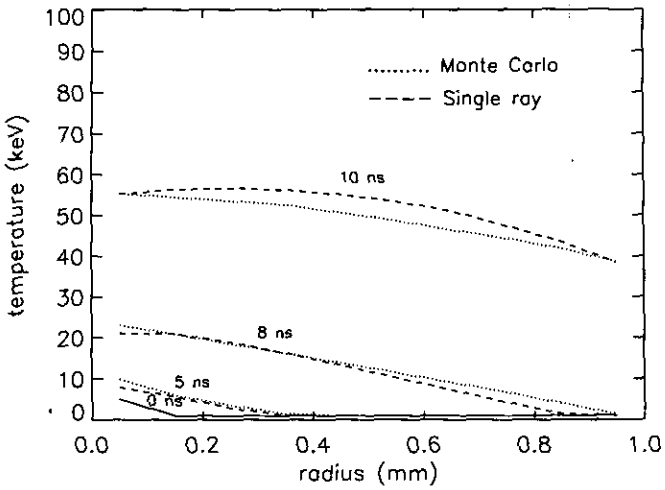

FIG. 3. As in Fig. 2, except for a DT cylinder of radius 1.0 mm.

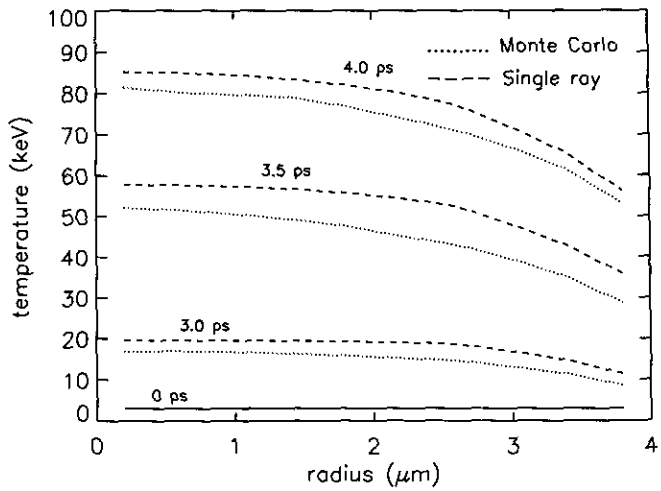

FIG. 5. As in Figs. 2 and 3, except for a DT sphere of radius 4.0 μm and density 3000 g cm^{-3}.

the temperature enhancement well, both spatially and temporally, in comparison to the more accurate Monte Carlo method. Timings of only the routines which perform the transport calculations revealed that for the planar case 550 seconds of CPU time was required for the Monte Carlo method on a Cray Y-MP. The single ray technique used only 0.1 s for the same calculation, a savings of over three orders of magnitude. This method is also expected to be considerably faster than multigroup diffusion, which, according to Ref. [2], is typically an order of magnitude faster than Monte Carlo. A specific comparison with an α transport calculation which employed multigroup diffusion is presented in Fig. 4. Corman *et al.* [2] considered a test case in spherical geometry in which the α's originate at the center of the sphere and distances are expressed in terms of λ_s, the distance over which the α's lose all their energy to electrons. Figure 4 shows the deposition to electrons in each zone at a temperature of 50 keV. The dotted line is the 100-group diffusion calculation presented in Fig. 9 of Ref. [2], and the solid line represents the results of the present treatment. The generally satisfactory agreement exhibited is similar to that shown in Ref. [2], where Monte Carlo is compared to multigroup diffusion. While no direct timing comparison with the 20-year-old calculation of Ref. [2] is feasible, it is obvious that the use of 10–100 energy groups in the diffusion calculation adds a corresponding computational burden not required in the present method, as explained in Section 2.2. Similar considerations apply when comparing the present transport method with S_n methods. In some respects, the spatial method of our technique is comparable to an S_n approach with $n = 2$; i.e., one accounts for particles flowing in the backward and forward directions along a ray. However, as discussed in Ref. [1], application of S_2 requires 6–12 energy groups.

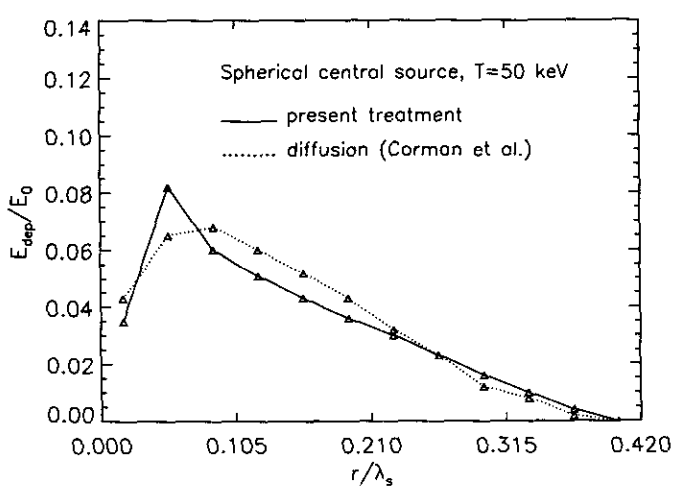

FIG. 4. Deposition of α's to electrons per zone is shown for a spherical central source of α particles, calculated both by the present method and by multigroup diffusion (Ref. [2]). The radius is normalized to the electron stopping distance, denoted by λ_s.

A spherical test case is presented in Fig. 5 for a much denser (3000 g cm^{-3}), smaller plasma (radius of 4.0 μm). In contrast to the planar and cylindrical cases, the temperature is assumed initially uniform at 3 keV. At such high densities, ignition and bootstrap heating occur on a timescale of picoseconds rather than nanoseconds. The outer edge remains coolest since the α particles can only be incident from 2π steradians, whereas in the interior the entire 4π solid angle can, in principle, be filled with α's. The temperature always maximizes at the center of the sphere due to its unique position, guaranteeing fully symmetric deposition by the α particles. This generates a large temperature gradient during burn, which the single-ray approximation is clearly capable of handling. The one-ray method has been found to give results similarly close to those of the Monte Carlo calculation for densities varying from a tenth of solid

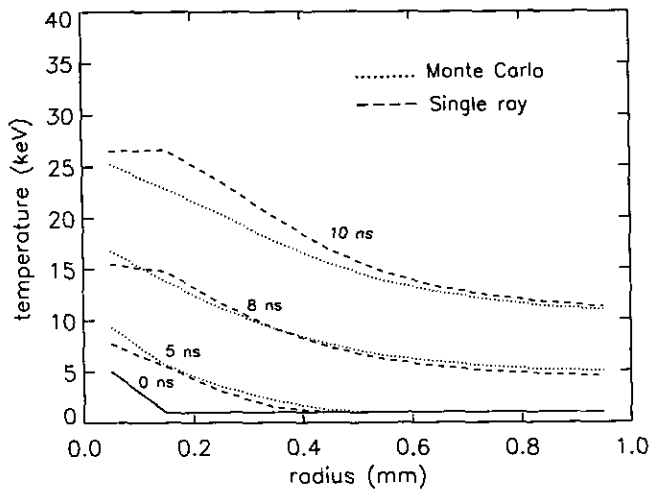

FIG. 6. As in Fig. 3, except that the density varies according to a Gaussian spatial profile, from 2.13 g cm^{-3} at the center of the cylinder to 0.0213 g cm^{-3} at its outer edge.

DT density to more than four orders of magnitude greater than that density.

The presence of a large density gradient does not significantly affect the accuracy of the single ray approximation, as shown in Fig. 6. As in Fig. 3, a cylinder is assumed whose central density is 10 times that of solid DT and whose radius is 1 mm. However, in this case, the density decreases according to a Gaussian spatial profile, as is also assumed in the Z pinch calculations of Ref. [8]. At the outer edge of the cylinder, the density has decreased to 1% of its central value. Note that the central temperature after 10 ns of burn is only about half that of the uniform-density cylinder of Fig. 3. The decreased density of the outer cells has produced fewer α particles to stream into and heat the central regions, hence the lower temperature of the variable density cylinder.

3.2. *Ignition Conditions in an Imploding Z Pinch*

One potentially fruitful application of the cylindrical version of the α transport methods described above is the problem of achieving ignition in a Z pinch. There are two general categories of Z pinches which have been considered as potential fusion reactors, the quasi-static Bennett-type pinch (see Refs. [8, 13] and references therein) and the imploding pinch (see Ref. [14] and references therein). The quasi-static pinch, including the effect of energy deposition by α particles has been analyzed in Ref. [13]. Assuming uniform current density, the Larmor radius of a 3.5 MeV alpha particle becomes significantly less than the pinch radius at currents of a few megamperes. Therefore, independent of the density and stopping power of the pinch plasma, some confinement of the α's is possible in any pinch likely to be suitable for fusion. If the current is confined to a skin depth at the exterior of the pinch, the α's will stream in straight lines in the interior and would be subject to collisional stopping as the principal confinement and energy extraction mechanism in that region. For very high uniform currents (>10 MA), the α particles are so tightly constrained by the magnetic field that the assumption of local deposition of the entire 3.5 MeV is reasonable. Recent experimental work by Kalantar and Hammer [7] supports the surface current picture. The absence of an interior magnetic field in such a pinch is conducive to the straight line trajectory approximation inside the pinch. However, Lovberg [8] finds that orbiting α's outside the pinch have a significant chance of re-entering the plasma and depositing more energy. The present calculations of alpha transport in an imploding pinch separately employ these contrasting pictures of current distribution to examine their effects. We do not consider re-entry of orbiting α's; in that sense, the calculation is conservative.

Reference [14] reviews the extensive existing diagnostics on imploding Z pinches. Although there is considerable scatter in the experimental data and uncertainty in the underlying theory, a picture of a "canonical" 1 MA Z pinch is presented which represents a rough consensus as to the conditions which such a pinch is capable of reaching. Final radii in the mm range, temperatures of several hundred electron volts, and total particle densities of a few times 10^{20} cm^{-3} are suggested. To achieve ignition assuming nanosecond confinement timescales, temperatures of several thousand electron volts, and densities of several times DT solid density are needed. Such conditions correspond to plasma pressures four orders of magnitude higher than those attained in a 1 MA imploding pinch. If one assumes similar final radii, a current approximately two orders of magnitude higher than 1 MA, i.e., 100 MA, would be required to reach ignition threshold via the simple implosion of a fusionable load. Such high current may be feasible, although a substantial advance over the present demonstrated maximum of 10 MA [15] is needed.

Our present calculation gives the time and spatial evolution of a 50-mg/cm Z pinch load consisting (by number) of 10% Al and 90% DT. We employ a 1D radiation MHD Lagrangian model [16]. Earlier work on phenomenological modeling of turbulence in Z pinches [17, 18] showed that the use of multipliers on the classical values of transport coefficients was needed to represent diagnostically inferred experimental conditions. Specifically, ion densities are reduced by orders of magnitude to good agreement with experiment by using enhanced transport. These enhanced values are: 30 times the classical conductivity and viscosity, and 20 times the classical resistivity. Other than these empirical adjustments, the model contains a comprehensive collisional-radiative description of the ionization dynamics as well as detailed radiation transport [9, 10].

The calculation is initiated with 93% of the mass uniformly distributed within a shell having a 1.25-cm inner radius and an outer radius of 1.75 cm. The remaining mass is distributed within six inner cells, with the density decreasing toward the axis. The driving current is sinusoidal with a quarter cycle of 55 ns and peak current of 120 MA. Calculations of poststagnation

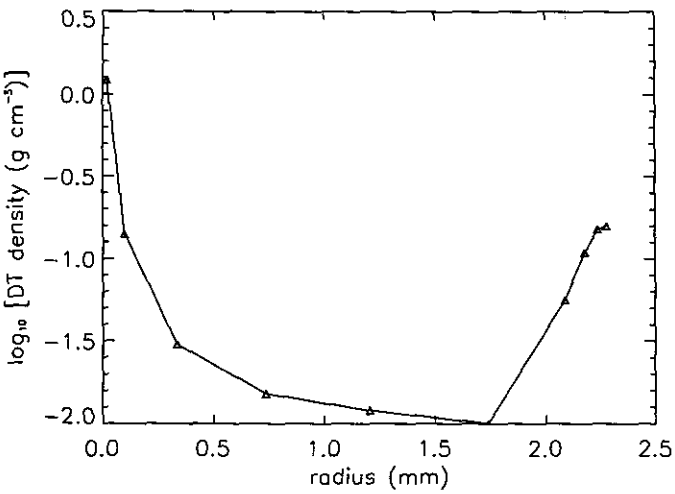

FIG. 7. DT density as a function of radius near peak compression during the implosion of a DT-Al plasma in a Z pinch driven by a peak current of 120 MA.

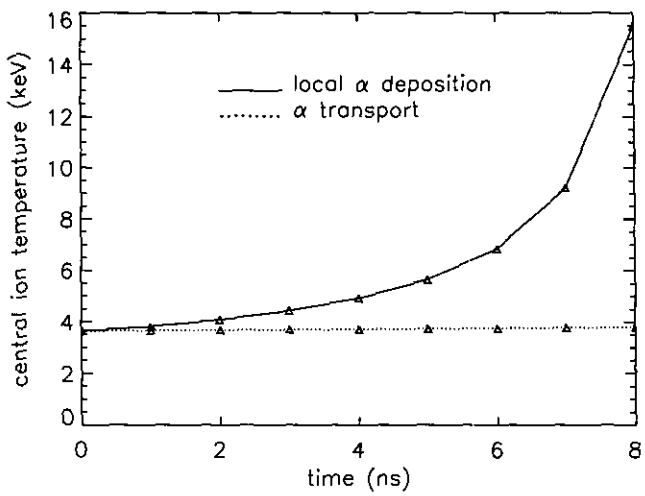

FIG. 9. Ion temperature vs. time in the central cell of the 120 MA DT–Al Z pinch is illustrated under the assumption of the fixed density profile given in Fig. 7. The solid line illustrates that, if all α particles are absorbed where produced, ignition occurs. In the free-streaming transport limit (dotted line) no ignition can occur.

current confinement of the plasma, as well as late time plasma heating, have not yet succeeded in reproducing experimental pinch behavior [19]. For this reason we terminate the current pulse when the outer radius of the pinch is within 0.35 cm of the axis. This is a conservative approach in the sense that the amount of energy that is available to heat the plasma during the stagnation phase of the implosion in limited to the amount of kinetic energy imparted to the plasma during the run-in. Also, we did not conduct a search for the smallest current needed for ignition by using innovative load design or current profiles. Therefore, 120 MA should not be interpreted as a minimum requirement.

The essential results of this study are shown in Figs. 7–9.

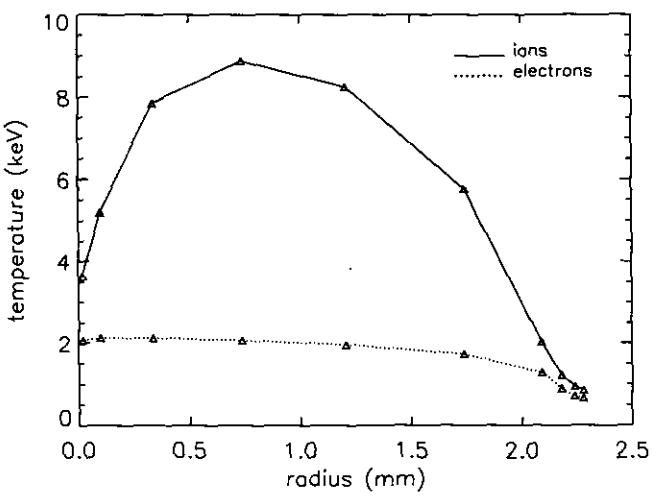

FIG. 8. As in Fig. 7, except that the ion and electron temperatures are illustrated.

The principal function of the Al is to allow greater compression of the plasma by radiating some of the energy and preventing excessive temperatures from terminating the implosion at too low a density. To some extent, density and temperature may be traded off by the use of such a seed material. As shown in Fig. 7, near peak compression the density on-axis of the DT component is about 1.2 g cm^{-3}, six times the solid density. According to Fig. 8, the ion temperature at the same point is 3.6 keV, nearly double the electron temperature. This illustrates an important facet of imploding Z pinches which is favorable to ignition. Prior to stagnation, the ions and electrons are travelling in an annulus toward $r = 0$ with about the same velocity, in this case about 6–7 $\times$ 10^7 cm s^{-1}. This velocity for the DT ions, if assumed randomized, corresponds to an ion temperature of 3–4 keV. At stagnation, when conversion to thermal energy occurs, the ions are thus initially hotter than the electrons. This specific ion heating mechanism cannot occur in a quasi-static single fiber pinch where no implosion occurs. However, in such pinches, Riley [20] has presented experimental evidence of ion temperatures exceeding that of the electrons and suggests turbulent heating as the cause. Figure 9 shows the result of a calculation which takes account of the subsequent heating by the α particles produced according to the profiles of Figs. 7 and 8 under the extreme assumptions (discussed above) of local deposition and free streaming. We caution that the density has been fixed in this part of the calculation to that given in Fig. 7. As discussed in Ref. [13], the α heating is likely to cause some re-expansion. Nevertheless, it is clear that the current distribution can critically influence the achievement of ignition through confinement of the α particles. According to Fig. 9, without the magnetic field internal to the pinch (which would

occur with current penetration), no ignition would occur in this scenario, since ρr alone is insufficient to extract the 3.5 MeV. Two caveats apply to this conclusion: we have ignored any possible effect of the Al ions in stopping the α's, and as previously mentioned, we also neglect repenetration of the α's orbiting the exterior of the pinch. The same figure reveals that complete confinement at very high current promotes bootstrap heating and ignition.

4. CONCLUDING REMARKS

The use of a single, or at most very few, representative paths to represent diffusive photon transport is ubiquitous, having been applied to laboratory plasmas, astrophysics, the Earth's atmosphere, and other media. In this paper we demonstrate that a similar technique holds some promise in simplifying the calculation of the fundamentally well-understood process of α particle transport in fusion plasmas. While the technique in its present form is not suitable for modeling scattering or bending of particle trajectories due to ambient magnetic fields, it is useful for simulations of a large class of plasmas having electron temperatures below 25 keV. Savings of CPU time of three orders of magnitude or more compared to a traditional Monte Carlo scheme is possible. In an initial application of the new method, we demonstrate with a specific Z pinch implosion a calculation that the attainment of ignition at a peak driver current of 120 MA may well depend on the details of any magnetic confinement of the α particles. This factor is directly related to the spatial current profile, whose details are just beginning to yield to experimental diagnosis.

ACKNOWLEDGMENTS

This work was supported by the Office of Naval Research.

REFERENCES

1. G. S. Fraley, E. J. Linnebur, R. J. Mason, and R. L. Morse, *Phys. Fluids* **17,** 474 (1974).
2. E. G. Corman, W. E. Loewe, G. E. Cooper, and A. M. Winslow, *Nucl. Fusion* **15,** 377 (1975).
3. R. S. Cooper and F. Evans, *Phys. Fluids* **18,** 332 (1975).
4. R. C. Kirkpatrick, *Nucl. Fusion* **21,** 1457 (1981).
5. R. L. McCrory and C. P. Verdon, "Inertial Confinement Fusion: Computer Simulation," in *Computer Applications in Plasma Science and Engineering*, edited by A. T. Drobot (Springer-Verlag, New York, 1991), p. 305.
6. R. D. Richtmeyer and K. W. Morton, *Difference Methods for Initial Value Problems* (Wiley, New York, 1967).
7. D. H. Kalantar and D. A. Hammer, *Phys. Rev. Lett.* **71,** 3806 (1993).
8. R. H. Lovberg, unpublished, 1990.
9. J. P. Apruzese, J. Davis, D. Duston, and K. G. Whitney, *J. Quant. Spectrosc. Radiat. Transfer* **23,** 479 (1980).
10. J. P. Apruzese, *J. Quant. Spectrosc. Radiat. Transfer* **25,** 419 (1981).
11. I. Carlvik, "A Method for Calculating Collision Probabilities in General Cylindrical Geometry and Applications to Flux Distributions and Dancoff Factors," in *Proceedings, Third International Conference on the Peaceful Uses of Atomic Energy, Vol. 2* (International Atomic Energy Agency, Vienna, 1965), p. 225.
12. S. Glasstone and R. H. Lovberg, *Controlled Thermonuclear Reactions* (Van Nostrand, New York, 1960), Chap. 2.
13. A. E. Robson, *Nucl. Fusion* **28,** 2171 (1988).
14. N. R. Pereira and J. Davis, *J. Appl. Phys.* **64,** R1 (1988).
15. R. B. Spielman *et al.*, *AIP Conf. Proc.* **195,** 3 (1989).
16. J. W. Thornhill, K. G. Whitney, and J. Davis, *J. Quant. Spectrosc. Radiat. Transfer* **44,** 251 (1990).
17. K. G. Whitney *et al.*, "Phenomenological Modeling of Argon Z Pinch Implosions," in *Proceedings, 9th International Conference on High-Power Particle Beams* (NTIS, Springfield, VA, 1993), p. 2044.
18. J. W. Thornhill, K. G. Whitney, C. Deeney, and P. D. LePell, *Phys. Plasmas* **1,** 321 (1994).
19. J. L. Giuliani *et al.*, *J. Quant. Spectrosc. Radiat. Transfer* **44,** 471 (1990).
20. R. A. Riley, Jr., Ph.D. thesis; Los Alamos National Laboratory Report LA-12722-T, 1994 (unpublished).